Conformational changes in the catalytically inactive nucleotide binding site of CFTR

László Csanády[1,2*], Csaba Mihályi[1], Andras Szollosi[1], Beáta Töröcsik[1], and Paola Vergani[3]

Running title: Movements in CFTR's degenerate site

[1]Department of Medical Biochemistry, Semmelweis University, Budapest, Hungary

[2]MTA-SE Ion Channel Research Group, Budapest, Hungary

[3]Department of Neuroscience, Physiology and Pharmacology, University College London, London, United Kingdom

*Correspondance:

Dr. László Csanády
Semmelweis University
Department of Medical Biochemistry
Tűzoltó u. 37-47
Budapest
H-1094, Hungary
E-mail: csanady.laszlo@med.semmelweis-univ.hu
Tel: (+36)-1-459-1500/60048
Fax: (+36)-1-267-0031

Abstract

A central step in the gating of the CFTR chloride channel is the association of its two cytosolic nucleotide binding domains (NBDs) into a head-to-tail dimer, with two nucleotides bound at the interface. Channel opening and closing, respectively, are coupled to formation and disruption of this tight NBD dimer. CFTR is an asymmetric ABC protein in which the two interfacial binding sites (composite sites 1 and 2) are functionally different. During gating the canonical, catalytically active, nucleotide binding site (site 2) cycles between dimerized prehydrolytic (state O_1), dimerized posthydrolytic (state O_2), and dissociated (state C) forms in a preferential $C \rightarrow O_1 \rightarrow O_2 \rightarrow C$ sequence. In contrast, the catalytically inactive nucleotide binding site (site 1) is believed to remain associated, ATP-bound, for several gating cycles. Here we have examined the possibility of conformational changes in site 1 during gating, by studying gating effects of perturbations in site 1.

Previous work showed that channel closure is slowed, both under hydrolytic and non-hydrolytic conditions, by occupancy of site 1 by N^6-(2-phenylethyl)-ATP (P-ATP) as well as by the site-1 mutation H1348A (NBD2 signature sequence). Here we found that P-ATP prolongs wild-type CFTR burst durations by selectively slowing (>2x) transition $O_1 \rightarrow O_2$, and decreases non-hydrolytic closing rate (transition $O_1 \rightarrow C$) of CFTR mutants K1250A (~4x) and E1371S (~3x). Mutation H1348A also slowed (~3x) the $O_1 \rightarrow O_2$ transition in the wild-type background, and decreased non-hydrolytic closing rate of both K1250A (~3x) and E1371S (~3x) background mutants. Neither P-ATP nor the H1348A mutation affected the 1:1 stoichiometry between ATP occlusion and channel burst events characteristic to wild-type CFTR gating in ATP. The marked effect different structural perturbations at site 1 have on both steps $O_1 \rightarrow C$ and $O_1 \rightarrow O_2$ suggests that the overall conformational changes CFTR undergoes upon opening, and coincident with hydrolysis at the active site 2, include significant structural rearrangement at site 1.

Keywords: dwell-time distribution, maximum likelihood, ABC-C family, free energy, nonequilibrium

Abbreviations: CFTR, Cystic Fibrosis Transmembrane Conductance Regulator; ABC, ATP-binding cassette; TMD, Transmembrane Domain; NBD, nucleotide-binding domain; WT, wild type; P_o, channel open probability; P-ATP, N^6-(2-phenylethyl)-ATP

Introduction

The Cystic Fibrosis Transmembrane Conductance Regulator (CFTR, ABCC7 (Riordan et al., 1989)) is a member of the asymmetric C subfamily of ATP Binding Cassette (ABC) proteins. Most ABC proteins are active transporters which move a variety of substrates across biological membranes. The substrate translocation pathway, formed by two transmembrane domains (TMDs), cycles between inward- and outward-facing conformations driven by an ATP hydrolysis cycle catalyzed by the two cytosolic nucleotide binding domains (NBDs). ABC NBDs contain three highly conserved sequence motifs: the Walker A (GXXXXGKS/T) and B (ΦΦΦΦDE, with Φ representing hydrophobic residues), and the ABC signature motif (LSGGQR/K). In each catalytic cycle ATP binding to the Walker motifs of both NBDs promotes formation of a tight head-to-tail NBD dimer which occludes two ATP molecules in composite interfacial catalytic sites formed by the Walker motifs of one NBD and the signature motif of the other. ATP hydrolysis is required to disrupt this dimer to allow nucleotide exchange and initiation of a new cycle (Hollenstein et al., 2007). Members of the C subfamily share this overall architecture, but show a marked asymmetry in the primary sequences of their two NBDs. Due to non-canonical substitutions in the Walker B and in other conserved motifs of the N-terminal NBD (NBD1) and in the signature sequence of the C-terminal NBD (NBD2) the catalytic site containing these motifs (site 1) is inactive (Aleksandrov et al., 2002; Basso et al., 2003), leaving ABC-C proteins with a single catalytically active site (site 2, formed by Walker motifs of NBD2 and signature sequence of NBD1). Non-canonical substitutions in the same key positions, resulting in reduced or absent hydrolysis at one composite site are also seen in the clinically important transporter associated with antigen processing (formed by TAP1 and TAP2, of the human ABC-B subfamily (Procko et al., 2009)), as well as numerous yeast and prokaryotic transporters (Szollosi et al., 2011). The latter group includes TM287/288, a heterodimeric transporter from *Thermotoga maritima* whose high resolution structure has been recently solved (Hohl et al., 2012).

CFTR, the protein mutated in cystic fibrosis patients (Riordan et al., 1989), is the only member of the ABC-C family whose TMDs are known to form the pore of a Cl^- ion channel. In addition to the canonical ABC domains CFTR contains a unique regulatory (R) domain, phosphorylation of which by cAMP-dependent protein kinase (protein kinase A, PKA) is a prerequisite for channel gating (Anderson

et al., 1991). In phosphorylated CFTR the pore opens to a burst upon ATP-induced dimerization of its NBDs and closes from a burst upon dimer dissociation (Vergani et al., 2005) following ATP hydrolysis at site 2; thus, in wild-type (WT) CFTR, each gating cycle (or burst of openings) is coupled to hydrolysis of one ATP molecule (Csanády et al., 2010). Deviations from this strict 1:1 coupling between ATP hydrolysis events and bursts of openings have been suggested to happen in mutants or in the presence of drugs. Catalytic site mutations can *lower* this coupling ratio leading to bursts that involve ATP occlusion/deocclusion but no hydrolysis (Csanády et al., 2010). In contrast, [ATP]-dependent prolongation of open burst durations for the W401F CFTR mutant (Jih et al., 2012b), or for WT CFTR gating in the presence of the potentiator compound Vx-770 (Jih and Hwang, 2013), have led to the suggestion that posthydrolytic ADP/ATP exchange in site 2 might occur without intervening pore closure, thereby *increasing* the coupling ratio by allowing more than one ATP to be hydrolyzed in site 2 within a single gating cycle (Jih et al., 2012a).

Biochemical work using γ-^{32}P-labeled ATP analogues revealed that ATP remains bound at CFTR's NBD1 for periods much longer (several minutes) than a channel gating cycle (~1 s), without being hydrolyzed (Aleksandrov et al., 2002; Basso et al., 2003). In a recent study (Tsai et al., 2010) nucleotide exchange time constants at the two sites were measured using a functional approach. The high-affinity ATP analogue N^6-(2-phenylethyl)-ATP (P-ATP) was found to speed opening and slow closing of CFTR channels, but the onset of these two effects following sudden replacement of ATP with P-ATP in the bath (cytosolic) solution followed distinct time courses. Whereas the effect on opening rate appeared instantaneously, suggesting it to be caused by P-ATP binding to the rapid-turnover site 2, the onset of slowed closure followed with a delay of 30-50 s, consistent with ATP/P-ATP exchange occurring more slowly at degenerate site 1. Furthermore, because nucleotide exchange rate at site 1 was affected by mutations in the NBD2 signature sequence – which completes site 1 only in a formed dimer – the authors suggested only partial separation of the NBD dimer in closed channels, the interface remaining closed around site 1 for several gating cycles. This notion obtained further support from thermodynamic studies (Szollosi et al., 2011) which examined state-dependent changes in energetic coupling between pairs of residues on opposing faces of the site 1 interface. A lack of change

in energetic coupling for three such pairs was interpreted to be consistent with the model suggested by Tsai and colleagues, i.e., with an "immobile" site 1 remaining closed throughout the gating cycle.

Nevertheless, site 1 clearly does play a role in gating energetics, as perturbations at site 1 can profoundly alter channel gating kinetics. For instance, the K464A mutation, which – by removing the side chain of the conserved NBD1 Walker A lysine – perturbs the NBD1-side of site 1, dramatically alters the mechanism of gating (Csanády et al., 2010). In addition, the H1348A mutation in the NBD2 signature sequence, which perturbs the NBD2-side of site 1, was found to slow channel closure (Szollosi et al., 2011). Finally, gating is affected by perturbations of the nucleotide structure at site 1, since P-ATP bound at site 1 also slows channel closure (Tsai et al., 2010). However, the exact mechanisms by which the H1348A mutation, or P-ATP bound at site 1, affect gating have not yet been elucidated. To gain further insight into the energetic consequences of perturbations at site 1, we examined in detail the effects of these two perturbations on CFTR channel gating. Our observations suggest that, despite maintained contact between residues on opposite sides of site 1, this site does not remain "frozen"; rather, significant conformational changes are likely to take place there both during channel opening, and concomitant with ATP hydrolysis at site 2.

Materials and methods

Molecular Biology

Human wild-type CFTR and CFTR segment 433-1480 in the pGEMHE plasmid (Chan et al., 2000) served as templates for mutants H1348A, K1250A, E1371S, K1250A/H1348A, E1371S/H1348A, E1371S/K464A, and 433-1480(K1250A) which were created using the QuikChange kit (Stratagene). The entire coding sequence of each construct was verified by automated sequencing (LGC Genomics). T7 polymerase was used for in vitro transcription (Ambion Mmessage Kit), and purified cRNA was stored at -80^{o}C.

Isolation and Injection of Xenopus Oocytes

Xenopus laevis oocytes were extracted and treated with collagenase as described (Chan et al., 2000), isolated oocytes were stored at 18 ^{o}C in a solution containing (in mM) 82 NaCl, 2 KCl, 1 $MgCl_2$, 5 Hepes (pH 7.5 with NaOH), 1.8 mM $CaCl_2$ and 50 μg/ml Gentamycin. To obtain expression levels appropriate for single-channel or macroscopic recordings, oocytes were microinjected with 0.1-10 ng of CFTR cRNA, and further incubated at 18 ^{o}C for 2-3 days.

Excised inside-out patch-clamp recordings

For inside-out patch recordings the pipette solution contained (in mM) 136 NMDG-Cl, 2 $MgCl_2$, 5 HEPES, pH=7.4 with NMDG. The bath solution was continuously flowing, and contained (in mM) 134 NMDG-Cl, 2 $MgCl_2$, 5 HEPES, 0.5 EGTA, pH=7.1 with NMDG. MgATP (Sigma) was added from a 400-mM aqueous stock solution (pH=7.1 with NMDG) to achieve a final concentration of 2 mM (or 10 mM for channels bearing the K1250A mutation). A 10 mM aqueous stock solution of N^6-(2-phenylethyl)-ATP (P-ATP) Na^+ salt (Biolog LSI) was stored at -80 ^{o}C, and diluted into the bath solution immediately before recording, to achieve a final concentration of 10 μM (or 50 μM for K1250A mutants). CFTR channels were fully activated by a 1-2 minute cytosolic exposure to 300 nM catalytic subunit of PKA (Sigma); all experiments shown were done in the partially dephosphorylated state following PKA removal, which remains stable over the time course of several minutes (Csanády et al., 2000). Switching between various bath solutions was achieved using computer-controlled

electronic valves (Heka); solution exchange time constant was 20-50 ms. Experiments were performed at 25 ^{o}C. Unitary CFTR currents were recorded (Axopatch 200B, Molecular Devices) at a pipette holding potential of +80 mV (V_m=-80 mV), filtered at 2 kHz, and digitized at 10 kHz (Digidata 1322A, Pclamp9, Molecular Devices). As CFTR gating is largely voltage-independent (Cai et al., 2003), macroscopic currents were recorded at membrane potentials between -20 mV and -80 mV.

Steady-state kinetic analysis of multichannel patches

Mean burst and interburst durations were extracted from steady segments of record with 1-6 active CFTR channels as described (Csanády et al., 2000). Currents were digitally filtered at 100 Hz, and idealized by half-amplitude threshold crossing. Events lists were fitted with a simple model in which ATP-dependent slow gating is pooled into a closed-open scheme and ATP-independent brief closures modeled as pore-blockage events (Ishihara and Welsh, 1997). Rate constants (r_{CO}, r_{OC}, r_{OB}, r_{BO}) of the resulting Closed-Open-Blocked (C↔O↔B) scheme were extracted by a simultaneous maximum likelihood fit to the dwell-time histograms of all conductance levels, while accounting for the filter dead time (Csanády, 2000). Mean burst duration was then calculated as $(1/r_{OC})(1+ r_{OB}/r_{BO})$ (Fig. 1F, Fig. 2C), and mean interburst duration as $1/r_{CO}$ (Fig. 1G, Fig. 2D). The estimates of interburst duration, and consequently of open probability (P_o), are sensitive to correct estimation of the number of channels (N) in the patch. These parameters were therefore used only if N could be determined with reasonable confidence; for this subset of patches N was ≤5.

To extract the gating pattern of channels loaded with either ATP or P-ATP at both sites, segments immediately following nucleotide exchange were not included in our analysis. The starting point for idealization was assigned individually for each patch, based on visual inspection, with analysis restricted to segments in which the gating pattern had already stabilized. The time required for stabilization following nucleotide exchange was typically between 10-60 s. To facilitate nucleotide loss from site 1, believed to happen faster in closed channels (Tsai et al., 2010), in some cases patches were rinsed with nucleotide-free solution for 20-30 s before applying a different nucleotide (e.g., Figs. 4, 6).

Burst analysis of single-channel patches

Burst analysis was done as described (Csanády et al., 2010). In brief, open bursts from records with a single active channel were isolated by ignoring closures shorter than a cutoff, chosen using the method of Jackson et al. (1983). The distributions of the durations of bursts obtained in this way were fitted using maximum likelihood (Colquhoun and Sigworth, 1995) to either a single-exponential distribution (Fig. 7A, B, *blue dotted lines*), or to the Scheme in Figure 7C with the slow rate k_{-1} fixed to 0 (Fig. 7A, B, *red solid lines*); events shorter than t_{low}=12 ms were excluded from the analysis. The probability density functions of the two fitted models are given by $f(k, t)=k\cdot\exp(-kt)$ and $f(k_1, k_2, t)=(k_1k_2/(k_2-k_1)) \cdot (\exp(-k_1t)-\exp(-k_2t))$, respectively; the improvement of the fit due to introduction of the second free parameter was evaluated using the log-likelihood ratio test, and found significant for both distributions in Figure 7A-B.

Analysis of macroscopic current relaxations

Macroscopic current decay time courses were fitted with single exponential functions using non-linear least squares (pClamp9), and closing rate defined as the inverse of the fitted time constant. For the non-hydrolytic mutants (K1250A, E1371S, and double mutants) the decay time courses following nucleotide removal often required a double exponential function – of the form $I(t)=I_0(A_1\exp(-t/\tau_1)+(1-A_1)\exp(-t/\tau_2))$ – with two slow time constants for a satisfactory fit (e.g., Fig. 3B, E), suggesting the presence of two populations of open-channel bursts. In such cases the average steady-state burst duration (τ^*) was estimated as $\tau^*=\tau_1\tau_2/(A_1\tau_2+A_2\tau_1)$, and average closing rate defined as $1/\tau^*$ (Szollosi et al., 2011).

Mutant Cycle Analysis

Mutant cycle analysis (Fersht, 2002) was used to give a measure of the energetic coupling ($\Delta\Delta G_{int}$) between pairs of target structural elements as described previously (Vergani et al., 2005; Szollosi et al., 2010; Szollosi et al., 2011). Briefly, perturbation-induced changes (between corners i and j of a mutant cycle) in activation free energy barriers ($\Delta\Delta G^{\ddagger}$) for closing were calculated from the changes in (hydrolytic and non-hydrolytic) closing rates (r) as $\Delta\Delta G^{\ddagger}_{j\text{-}i}=-RT\ln(r_j/r_i)$, and $\Delta\Delta G_{int}$ defined

as the difference between $\Delta\Delta G^{\ddagger}$ values along parallel sides of the mutant cycle (e.g., $\Delta\Delta G^{\ddagger}_{4\text{-}3} - \Delta\Delta G^{\ddagger}_{2\text{-}1}$). All ΔGs are given as mean ± SEM. Since the numbers of observations, N, for each corner of the cycle are similar, SEMs were calculated using the mean value for N.

Statistics

Data are given as mean±SEM of at least 5 measurements. Statistical significance was evaluated using Student's t-test (*$P<0.05$; **$P<0.01$).

Online Supplemental Material

Figure S1 compares single-channel conductances in ATP vs. P-ATP. Figure S2 shows the effect of the K464A mutation on non-hydrolytic closing rate measured in the E1371S background.

Results

P-ATP stimulates CFTR channel opening with high affinity, and prolongs steady-state burst durations

We first determined rough kinetic parameters for CFTR channels gating in P-ATP in our experimental system. Apparent affinities for ATP and P-ATP were compared in macroscopic patches by applying test concentrations of the nucleotide bracketed by applications of a saturating (2 mM, and 32 μM, respectively) concentration (Fig. 1A-B). Fractional currents plotted against nucleotide concentration (Fig. 1C) were well fit by the Michaelis-Menten equation and yielded K_m values of 40±2 μM for ATP (Fig. 1C, blue), but 2.4±0.2 μM for P-ATP. We next compared steady-state gating of CFTR channels exposed either to a close-to-saturating concentration of 10 μM P-ATP or to 2 mM ATP, in patches containing a few (≤2) channels in which individual gating transitions remained clearly resolved (Fig. 1D). Kinetic analysis (see Methods) revealed significantly higher open probability (P_o) in P-ATP as compared to that seen in ATP (Fig. 1E), which was largely caused by ~2-fold longer mean burst durations (Fig. 1F) together with a small reduction in interburst durations (Fig. 1G). These results confirm earlier studies which have established P-ATP as a high-affinity, potent CFTR stimulator (Zhou et al., 2005; Tsai et al., 2010).

[ATP] does not affect the prolongation of steady state burst duration by the H1348A mutation

In an earlier study we found that the H1348A mutation prolongs burst durations of CFTR channels gating in 2 mM ATP by ~3-fold (Szollosi et al., 2011). Because for another site-1 mutant (W401F) mean burst durations were shown to increase at high millimolar ATP concentrations (Jih et al., 2012b), we tested whether that was the case for H1348A CFTR. However, comparing the patterns of gating in 2 mM and 10 mM ATP (Fig. 2A) did not reveal any significant effect of raising [ATP] above 2 mM; kinetic analysis revealed identical P_o (Fig. 2B), mean burst (Fig. 2C) and interburst (Fig. 2D) durations under these two conditions.

Both P-ATP and the H1348A mutation slow non-hydrolytic channel closure

To quantitatively compare the effects of our site-1 perturbations on the slow rate of non-hydrolytic closure we studied macroscopic closing rates following nucleotide removal for channels in

which nucleotide hydrolysis at site 2 is abrogated by mutagenesis. Because different NBD2 mutations, in addition to disrupting ATP hydrolysis, likely differentially alter the stability of the open state, we do not know which non-hydrolytic mutant is the best model for the O_1 state of WT CFTR. We therefore compared the effects of our site-1 perturbations on the closing rates of two non-hydrolytic mutants, NBD2 Walker A mutant K1250A (Fig. 3A-C), and NBD2 Walker B mutant E1371S (Fig. 3D-F). Both P-ATP (Fig. 3A, D, *red fit lines* and *time constants*) and the H1348A mutation (Fig. 3B, E, *green fit lines* and *time constants*) caused markedly slower current relaxations than those observed for the two background constructs upon removal of ATP (Fig. 3A, D, *blue fit lines* and *time constants*; cf., (Zhou et al., 2005; Szollosi et al., 2011). Thus, non-hydrolytic closing rate (Fig. 3C, F, *bars*; calculated from the fitted relaxation time constants as described in Methods) was similarly affected by both site-1 perturbations, and this was true regardless of whether the K1250A (Fig. 3C) or the E1371S (Fig. 3F) mutant was chosen as the non-hydrolytic model; i.e., both site-1 perturbations decreased this rate by 2-3-fold.

Non-additive effects of P-ATP and site-1 mutations on hydrolytic closure support slowing of this gating step by P-ATP bound in site 1

Slowing of both hydrolytic and non-hydrolytic closure by P-ATP was suggested to result from occupation of site 1 by this nucleotide, based on the delayed onset of both effects following application of the analogue (Tsai et al., 2010). We used thermodynamic mutant cycles (Fersht, 2002) as an independent approach to test this hypothesis. Non-additive effects on gating of two structural perturbations suggest that those two structural elements are energetically coupled. Channels opened by P-ATP contain two structural "perturbations": a phenylethyl group (P-group) linked to N^6 of the adenine of the nucleotide bound in site 1, and another P-group on the nucleotide bound in site 2. If the presence of the P-group in site 2 affects closing rate, then this effect is expected to be additive with effects on closing rate of mutations in the spatially distant site 1. In contrast, if the P-group in site 1 is responsible for the effects of P-ATP on closing, then P-ATP and mutations of site-1 residues (which are energetically coupled to this P-group) will affect closing rate in a non-additive manner. We chose two site-1 perturbations to test for additivity of effects on closing rate with those of P-ATP. On the

NBD2 side of site 1 we chose mutation H1348A, because this perturbation causes a large effect on closing rate in ATP which we had already characterized (Fig. 2). To perturb the NBD1-side of site 1, we chose to delete most of a non-conserved insertion in CFTR's NBD1 (called the "regulatory insertion", RI (Lewis et al., 2004)) by co-expression of CFTR segments 1-414 and 433-1480. This "ΔRI" perturbation leaves ATP-dependent gating largely intact (Csanády et al., 2005), but is nevertheless expected to cause local distortion in areas of NBD1 which contact the adenine base of the site-1-bound nucleotide.

We first characterized the effect of P-ATP on hydrolytic closing rate in these two mutant backgrounds (Fig. 4) by recording single-channel activity of H1348A (Fig. 4A), or of ΔRI channels (Fig. 4D), alternately exposed to either 2 mM ATP (Fig. 4A, D, *green segments*) or 10 μM P-ATP (Fig. 4A, D, *brown segments*). Consistent with previous work, the H1348A and ΔRI perturbations differentially affected hydrolytic closure: closing rate in ATP was unchanged for ΔRI (Fig. 4E, compare *green bar* with *blue bar*; cf., (Csanády et al., 2005)), but 2-3-fold slowed for H1348A (Fig. 4B, compare *green bar* with *blue bar*; cf., Fig. 2C). However, switching from ATP to P-ATP (Fig. 4A, D, *brown segments*) did not elicit any noticeable change in the length of channel open bursts for either construct (Fig. 4A, D, compare *brown* with *green segments* in expanded *insets*). Thus, P-ATP does not slow hydrolytic closure when applied in the H1348A or ΔRI mutant background (Fig. 4B, E, compare *brown* with *green bars*). Although the 2-fold effect of P-ATP on hydrolytic closing rate of WT CFTR is small in energetic terms, the difference in the effects of the mutations on closing rates in P-ATP vs. in ATP yielded interaction free energies ($\Delta\Delta G_{int(closing)}$) – both between the P-group and residue 1348 (Fig. 4C) and between the P-group and the RI region (Fig. 4F) – which were significantly different from zero ($P<0.05$). This is consistent with the effect on hydrolytic closing rate being caused by the P-group in site 1.

Non-additive effects of P-ATP and site-1 mutations on non-hydrolytic closure support slowing of this gating step by P-ATP bound in site 1

Additivity of effects on non-hydrolytic closure of the same site-1 perturbations with those of P-ATP were tested in the K1250A non-hydrolytic background (Figure 5), by measuring macroscopic

closing rate of K1250A/H1348A channels (Fig. 5A), and of channels obtained by co-expression of segments 1-414 and 433-1480(K1250A) (K1250A/ΔRI, Fig. 5D) upon nucleotide removal. The H1348A and ΔRI perturbations affected non-hydrolytic closing rate in opposite ways: whereas mutation H1348A slowed it by ~3-fold (Fig. 5B, compare *green bar* with *blue bar*; cf., Fig. 3C) the ΔRI perturbation accelerated it ~3-fold (Fig. 5E, compare *green bar* with *blue bar*; cf., (Csanády et al., 2005)). Interestingly, neither perturbation abolished the effect of P-ATP on non-hydrolytic closure (Fig. 5A, D, compare *brown* with *green* single-exponential *fit lines* and *time constants*): rather, both perturbations seemed to potentiate it. Thus, whereas P-ATP slowed non-hydrolytic closure by ~4-fold for K1250A channels with an intact site 1 (Fig. 3C, compare *red* with *blue bar*; replotted in Fig. 5B, E), this effect increased to >6-fold, and to ~9-fold, respectively, in the presence of the site-1 perturbations H1348A and ΔRI (Fig. 5B, E, compare *brown* with *green bars*), again suggesting non-additivity. Indeed, mutant cycles built on non-hydrolytic closing rates (Fig. 5C, F) yielded interaction free energies between the P-group and residue 1348 (Fig. 5C), as well as between the P-group and the RI region (Fig. 5F), significantly different from zero ($P<0.05$ and $P<0.01$, respectively), consistent with the effect on non-hydrolytic closing rate also being caused by the P-group in site 1.

Neither P-ATP nor the H1348A mutation disrupts near 1:1 stoichiometry between ATP occlusion and channel burst events

Both P-ATP and the H1348A mutation prolong steady-state mean burst durations (Figs. 1F and 2C). Recent studies suggested a novel mechanism for a prolongation of steady-state CFTR burst durations for NBD1 mutant W401F (Jih et al., 2012b; Jih et al., 2012a), by proposing the presence of a short time window at the end of each burst during which the hydrolysis products ADP and phosphate at site 2 can be replaced by a new ATP molecule without intervening channel gate closure. Such a "reentry" mechanism should allow for more than one ATP hydrolysis cycle to happen within a single burst, thereby prolonging the mean duration of bursts at steady state. A simply testable prediction of such a model is a discrepancy between the burst durations measured at steady-state, and the time constant of the macroscopic current relaxation following sudden removal of ATP. This is because the latter closing rate is measured under conditions which preclude a reentry cycle, i.e., in the absence of

nucleotides. Because the W401F mutation also resides in site 1, we asked whether a reentry mechanism might explain the longer burst durations in P-ATP or in the presence of the H1348A mutation. To this end, we measured macroscopic closing rates following nucleotide removal for WT and ΔRI channels opened by either 2 mM ATP or by 10 μM P-ATP (Fig. 6A, C), and for H1348A channels opened by 2 or 10 mM ATP (Fig. 6B, *top*) or by 10 μM P-ATP (Fig. 6B, *bottom*). Current relaxation time courses were fitted by single exponentials (*colored lines*). The time constants of these exponentials reflect the mean duration of bursts which do not contain reentry events. When we compared these time constants (Fig. 6D, *colored bars*) with the steady-state mean burst durations measured in the presence of the respective nucleotide (Fig. 6D, *striped bars*, data replotted from Figs. 1F, 2C, 4B, and 4E), we found in each case a very close agreement; importantly, in no case was the steady-state burst duration longer than the macroscopic estimate. This suggests that both for WT (and ΔRI) channels gating in P-ATP, and for H1348A channels gating in 2 or 10 mM ATP or 10 μM P-ATP, each steady-state burst involves occlusion of a single nucleotide at site 2, just as suggested for WT channels gating in ATP (Csanády et al., 2010).

Of note, enhancement of macroscopic WT CFTR current by P-ATP, relative to ATP, was slightly smaller (<1.5-fold; see Fig. 6A) than expected from the fractional increase in P_o (~1.55-fold; Fig. 1E). This small discrepancy is accounted for by the slightly smaller average conductance of channels opened by P-ATP, which likely reflects rapid flickery closures not fully resolved at our recording bandwidth (Fig. S1). Thus, at -80 mV, average unitary current of open channels was -0.59±0.01 pA (n=6) in ATP, but significantly (P<0.01) smaller, -0.55±0.01 pA (n=6), in P-ATP.

Both P-ATP and the H1348A mutation prolong bursts by slowing the $O_1 \rightarrow O_2$ transition

Thus, under the conditions studied here, the duration of each open burst includes some time spent in a pre-hydrolytic open state (O_1, Fig. 7C), in which a nucleoside triphosphate is occluded at site 2, followed by a shorter time interval in a less stable posthydrolytic open state (O_2, Fig. 7C). Because the rate (k_{-1}) of non-hydrolytic closure (step $O_1 \rightarrow C_1$, Fig. 7C) is very slow (see Fig. 3), the overall mean burst duration is mostly determined by the rates of the $O_1 \rightarrow O_2$ and $O_2 \rightarrow C_2$ transitions (k_1 and k_2, Fig. 7C). The latter two rates can be estimated by fitting the scheme in Figure 7C to the distributions of

open burst durations using maximum likelihood (Colquhoun et al., 1995). To determine which of these two rates are affected by P-ATP and the H1348A mutation, respectively, we recorded currents from patches containing a single active channel (Fig. 7A-B, *insets*). Open burst events were isolated by burst analysis (see Methods), pooled from several patches, and fitted by maximum likelihood. The histograms of burst durations were distinctly peaked for both WT channels gating in 10 μM P-ATP (Fig. 7A) and H1348A channels gating in 2 mM ATP (Fig. 7B), consistent with a nonequilibrium gating cycle which involves nucleotide hydrolysis. The most striking difference between these distributions and that found earlier for WT channels gating in ATP (Csanády et al., 2010) was in the tail, which was distinctly longer in the presence of the site-1 perturbations, whereas the positions of the peaks were little moved. Accordingly, the maximum likelihood fit yielded 2-3-fold slower k_1 values (Fig. 7D, *left*) in the presence of P-ATP (*red bar*) or the H1348A mutation (*green bar*) compared to the earlier estimate for WT channels gating in ATP (*blue bar*, replotted from (Csanády et al., 2010). In contrast, neither P-ATP nor the H1348A mutation seemed to dramatically affect the faster rate k_2 (Fig. 7D, *right*).

Discussion

In this study we have investigated in detail the effects on channel gating of two structural perturbations at CFTR's degenerate interfacial ATP binding site (site 1). The H1348A mutation removes a histidine side chain from the signature sequence of NBD2, thereby perturbing the NBD2-side of site 1, whereas the use of P-ATP introduces a phenylethyl group into this composite binding site. Although in our experiments, which involved prolonged exposure to P-ATP, both composite sites were presumably loaded with this ATP analogue, an elegant study by Tsai and colleagues (Tsai et al., 2010) convincingly demonstrated that the effect of P-ATP on burst length (cf., Fig. 1F) is due to the P-ATP molecule bound at site 1, whereas P-ATP bound at site 2 is responsible for the high-affinity potent stimulation of opening rate (cf., Fig. 1B-C). In addition, experiments using the non-hydrolyzable ATP analog AMPPNP together with P-ATP to lock WT channels in the open state suggested that the slowing of non-hydrolytic closure by P-ATP is also attributable to P-ATP bound at site 1 (Zhou et al., 2005). Here we provide further independent support for this assignment, by demonstrating non-additive effects on both hydrolytic and non-hydrolytic closing rate of P-ATP and of mutations on either face of composite site 1 (Figs. 4-5). Furthermore, combining maximum likelihood fitting of steady-state single-channel records with the analysis of macroscopic current relaxations, we have determined which microscopic rates are affected by these site-1 perturbations resulting in the increased stability of channel open states.

In two recent studies Jih and colleagues proposed the existence of a short time window at the end of each burst, which would follow the release of hydrolysis products from site 2 but precede gate closure, and allow a new ATP molecule to bind at site 2 returning the channel into a new prehydrolytic open state, without intervening gate closure. They further proposed that mutations or pharmacological modulation might prolong CFTR channel bursts by increasing the frequency of such "reentry" events (Jih et al., 2012b; Jih et al., 2012a; Jih et al., 2013). Because one such mutation (W401F) resides in site 1, we have evaluated the possibility that the H1348A mutation, or P-ATP bound in site 1, might also act by such a mechanism. However, the lack of effect of increasing [ATP] on steady-state burst durations of H1348A CFTR (Fig. 2C), and the close agreement of macroscopic closing time constants upon nucleotide removal with steady-state mean burst durations (Fig. 6) ruled out this possibility, and

confirmed that the two site-1 perturbations studied here do not disrupt the near 1:1 stoichiometry between ATP occlusion events and pore opening events, characteristic to WT CFTR gating in ATP (Csanády et al., 2010). Although comparison of macroscopic and steady-state closing rates (Fig. 6) might not be sensitive enough to rule out slight deviations from 1:1 stoichiometry, it is clear that small effects would not be sufficient to explain the 2-3-fold prolongation of burst durations by the H1348A mutation and P-ATP. We have therefore used a simplified cyclic scheme (Fig. 7C) as a framework for interpreting our kinetic results and have dissected the effects of site-1 perturbations on the three rates which determine the stability of the open states: those of steps $O_1 \rightarrow O_2$, $O_1 \rightarrow C_1$, and $O_2 \rightarrow C_2$ (Fig. 7C).

Interestingly, the detailed kinetic consequences of these two perturbations turned out to be very similar, amounting to a simultaneous 2-3-fold decrease in the rates of steps $O_1 \rightarrow O_2$ and $O_1 \rightarrow C_1$. This phenotype affords a simple explanation in terms of the free energy profile of the CFTR gating cycle (Fig. 8, *blue energy profile*). For a structural perturbation which selectively stabilizes the O_1 state, relative to both states C_1 and O_2 (by $\delta\Delta G_{O1}$; Fig. 8, *red energy profile*), a simultaneous increase in the heights of the transition-state barriers for both step $O_1 \rightarrow O_2$ ($\Delta G^{\ddagger}_1$; Fig. 8) and step $O_1 \rightarrow C_1$ ($\Delta G^{\ddagger}_{-1}$) is expected (compare *red* and *blue* vertical double-arrows in Fig. 8), resulting in slowed rates k_{-1} and k_1, as observed. In addition, the distortion of the energy profile, as drawn, also suggests a lower energy barrier for step $C_1 \rightarrow O_1$, predicting an increase in opening rate. Interestingly, this is exactly what we observed for the H1348A mutant, the opening rate of which is ~2-fold increased relative to WT (compare Fig. 2D, *green bar*, and Fig. 1G, *blue bar*). We also observed a more modest increase in WT opening rate in the presence of 10 μM (subsaturating) P-ATP (compare *red* and *blue bar* in Fig. 1G), but interpretation of this small effect is limited by the fact that stimulation of opening rate by P-ATP has been mostly attributed to P-ATP bound at site 2 (Tsai et al., 2010).

From an energetic point of view the effects of the site-1 perturbations we have studied are modest, on the order of ~1 kT. However, two facts have to be considered when interpreting these effects. First, the measured $\Delta\Delta G$ values by no means represent the overall energetic change of the site-1 structure between states C_1 and O_1, or O_1 and O_2, but the change in environment of a single chemical moiety (the histidine side chain at position 1348, or the phenylethyl group of P-ATP in site 1) associated with those gating transitions. Second, our $\Delta\Delta G$ values reflect changes in barrier heights,

which suggest larger changes between ground states (see Fig. 8); e.g., an ~1 kT change in the barrier height for non-hydrolytic closure might be associated with a $\Delta\Delta G$ of ~2 kT between states C_1 and O_1. (As a comparison, $\Delta\Delta G_{int}$ between C_1 and O_1 is ~2 kT for residues 555 and 1246 on opposing faces of the active site 2 which completely separates during the $O_1 \rightarrow C_1$ transition (Vergani et al., 2005).)

What mechanistic insight can be gained from these observations? The recent suggestion that composite site 1 of CFTR does not separate upon channel closure (Tsai et al., 2010; Szollosi et al., 2011) has fostered a view of the degenerate site as a simple rigid scaffold, which does not participate in the functional movements of asymmetric ABC-C proteins (although this proposal has remained a matter of contention, (Chaves and Gadsby, 2011)). Our present data are hard to reconcile with such an assignment. The fact that removal of the histidine side chain at position 1348 selectively stabilizes state O_1 relative to C_1 (Fig. 8) is most simply explained by postulating that in the WT channel the environment of that histidine side chain is not identical in those two states. The similar effect of P-ATP bound at site 1 suggests that the phenylethyl group also experiences a change in environment during the $C_1 \leftrightarrow O_1$ transition. It follows then that significant movement is likely to take place at site 1 during the channel opening step, even if the composite site does not actually separate in a closed channel. Furthermore, the selective energetic stabilization of state O_1 relative to O_2 (Fig. 8) by both perturbations implies that in a WT channel the physico-chemical environment of the H1348A side chain, or of the phenylethyl group of a P-ATP molecule bound at site 1, experiences a significant change also during the $O_1 \rightarrow O_2$ transition, i.e., upon ATP hydrolysis at the active composite site 2. The implication is a significant movement in site 1 upon ATP hydrolysis at site 2: a classical allosteric effect. Interestingly, the K464A mutation, which perturbs site 1 by removing the conserved Walker A lysine was also shown to affect the energetics of both of the $C_1 \leftrightarrow O_1$ and $O_1 \rightarrow O_2$ gating steps (Csanády et al., 2010), although in a different way: in this mutant rate k_1 decreased ~4-fold, while the rate of non-hydrolytic closure, in a K1250A mutant background, increased by ~10-fold (this is also replicated in the E1371S background, Fig. S2). Thus, although the distortion of the energetic profile by the K464A mutation differs from that seen for the two perturbations studied here, the K464A result is again consistent with movements in site 1 occurring in both of the above gating steps.

In principle, we cannot exclude the possibility of a "static allosteric effect" as an alternative scenario to explain our results. That is, perturbations in site 1 might statically impose a slightly different overall conformation of the NBDs which leads to altered transition rates associated with reactions and conformational changes occurring at the active site 2, without movements in site 1 during those transitions. However, such an interpretation is at odds with the generally accepted view of protein allostery. Thus, manipulations at one site in a protein (the "allosteric site") which affect conformational changes at a distant site (the "active site") generally involve movement at the allosteric site itself: allosteric modulators affect the conformational equilibrium of proteins because the affinity of their binding sites changes during the conformational transition. Examples range from BPG- or proton-modulation of oxygen binding in hemoglobin (Monod et al., 1965) to activation of ligand-gated channels (Changeux and Edelstein, 2005) – in contrast we are not aware of any example of a "frozen" allosteric site. We therefore feel that a conventional "dynamic allosteric effect", which involves movements in site 1 of CFTR, is a more likely explanation of our findings.

Does site 1 separate then, or not, during a normal gating cycle? The answer might lie somewhere in between. The recent determination of the TM287/288 structure (Hohl et al., 2012) at least suggests such an intermediate scenario. In this structure the transmembrane domains are seen in an inward-facing orientation, generally believed to correspond to the closed channel state in CFTR. At the same time, the NBD dimer interface is only partially separated (Fig. 9): the active site 2 is open and devoid of nucleotide (Fig. 9, *top composite site*), while the degenerate site (Fig. 9, *bottom composite site*) contains a bound AMPPNP molecule, and in it the opposing faces remain in contact. In particular, the α-carbons of an asparagine in the TM288 D-loop (Asn521 Fig. 9, *violet spacefill*) and that of a conserved threonine in the TM287 Walker A loop (T368 Fig. 9, *red spacefill*) are separated by only 5.7 Å, and the asparagine is seen to make contact with the γ-phosphate of the bound AMPPNP. Interestingly, the corresponding positions in site 1 of CFTR formed one of three interface pairs (T460-H1375) for which a lack of state-dependent changes in energetic coupling was interpreted to suggest a maintained interaction throughout the gating cycle (Szollosi et al., 2011). However, consistent with the data we present here, a comparison between TM287/288 and crystals with tightly dimerized NBDs highlights clear differences in composite site 1 structure. The distance between the Walker A motif and

the opposing signature sequence of the degenerate site is larger by ~3 Å in the TM287/288 structure (Hohl et al., 2012) than seen in tight dimers of ABC NBDs (e.g.; (Smith et al., 2002; Dawson and Locher, 2007)). The TM287/288 structure therefore also suggests some opening, although not complete separation, of the degenerate site.

In conclusion, the data presented here strongly suggest that significant movements occur in CFTR's composite site 1 concomitant with gating conformational changes. The precise extent and direction of these movements awaits further structural and functional studies.

Acknowledgements

We thank Dorottya Mayer for oocyte isolation and injection. Supported by NIH grant R01-DK051767, MTA Lendület grant LP2012-39/2012, and an International Early Career Scientist grant from the Howard Hughes Medical Institute to L.C.

References

Aleksandrov,L., A.A.Aleksandrov, X.B.Chang, and J.R.Riordan. 2002. The First Nucleotide Binding Domain of Cystic Fibrosis Transmembrane Conductance Regulator Is a Site of Stable Nucleotide Interaction, whereas the Second Is a Site of Rapid Turnover. *J Biol Chem* 277:15419-15425.

Anderson,M.P., D.P.Rich, R.J.Gregory, A.E.Smith, and M.J.Welsh. 1991. Generation of Camp-Activated Chloride Currents by Expression of Cftr. *Science* 251:679-682.

Basso,C., P.Vergani, A.C.Nairn, and D.C.Gadsby. 2003. Prolonged nonhydrolytic interaction of nucleotide with CFTR's NH2-terminal nucleotide binding domain and its role in channel gating. *J Gen Physiol* 122:333-348.

Cai,Z., T.S.Scott-Ward, and D.N.Sheppard. 2003. Voltage-dependent gating of the cystic fibrosis transmembrane conductance regulator Cl- channel. *J Gen Physiol* 122:605-620.

Chan,K.W., L.Csanády, D.Seto-Young, A.C.Nairn, and D.C.Gadsby. 2000. Severed molecules functionally define the boundaries of the cystic fibrosis transmembrane conductance regulator's NH(2)-terminal nucleotide binding domain. *J Gen Physiol* 116:163-180.

Changeux,J.P. and S.J.Edelstein. 2005. Allosteric mechanisms of signal transduction. *Science* 308:1424-1428.

Chaves,A.L. and D.C.Gadsby. 2011. Extent of Nucleotide-Binding Domain (NBD) Separation When a CFTR Channel Closes. *Biophysical Journal* 100:265-266.

Colquhoun,D. and F.J.Sigworth. 1995. Fitting and statistical analysis of single-channel records. *In* Single channel recording. B.Sakmann and E.Neher, editors. *Plenum Press*, New York.

Csanády,L. 2000. Rapid kinetic analysis of multichannel records by a simultaneous fit to all dwell-time histograms. *Biophys J* 78:785-799.

Csanády,L. 2006. Statistical evaluation of ion-channel gating models based on distributions of LogLikelihood Ratios. *Biophys J* 90:3523-3545.

Csanády,L., K.W.Chan, A.C.Nairn, and D.C.Gadsby. 2005. Functional roles of nonconserved structural segments in CFTR's NH2-terminal nucleotide binding domain. *J Gen Physiol* 125:43-55.

Csanády,L., K.W.Chan, D.Seto-Young, D.C.Kopsco, A.C.Nairn, and D.C.Gadsby. 2000. Severed channels probe regulation of gating of cystic fibrosis transmembrane conductance regulator by its cytoplasmic domains. *J Gen Physiol* 116:477-500.

Csanády,L., P.Vergani, and D.C.Gadsby. 2010. Strict coupling between CFTR's catalytic cycle and gating of its Cl- ion pore revealed by distributions of open channel burst durations. *Proc Natl Acad Sci U S A* 107:1241-1246.

Dawson,R.J.P. and K.P.Locher. 2007. Structure of the multidrug ABC transporter Sav1866 from Staphylococcus aureus in complex with AMP-PNP. *Febs Letters* 581:935-938.

Fersht,A. 2002. Structure and Mechanism in protein science. 4 ed. W.H.Freeman and Company, New York.

Hohl,M., C.Briand, M.G.Grutter, and M.A.Seeger. 2012. Crystal structure of a heterodimeric ABC transporter in its inward-facing conformation. *Nature Structural & Molecular Biology* 19:395-402.

Hollenstein,K., R.J.Dawson, and K.P.Locher. 2007. Structure and mechanism of ABC transporter proteins. *Curr Opin Struct Biol* 17:412-418.

Ishihara,H. and M.J.Welsh. 1997. Block by MOPS reveals a conformation change in the CFTR pore produced by ATP hydrolysis. *Am J Physiol* 273:C1278-C1289.

Jackson,M.B., B.S.Wong, C.E.Morris, H.Lecar, and C.N.Christian. 1983. Successive openings of the same acetylcholine receptor channel are correlated in open time. *Biophys J* 42:109-114.

Jih,K.Y. and T.C.Hwang. 2013. Vx-770 potentiates CFTR function by promoting decoupling between the gating cycle and ATP hydrolysis cycle. *Proc Natl Acad Sci U S A* 110:4404-4409.

Jih,K.Y., Y.Sohma, and T.C.Hwang. 2012a. Nonintegral stoichiometry in CFTR gating revealed by a pore-lining mutation. *Journal of General Physiology* 140:347-359.

Jih,K.Y., Y.Sohma, M.Li, and T.C.Hwang. 2012b. Identification of a novel post-hydrolytic state in CFTR gating. *Journal of General Physiology* 139:359-370.

Lewis,H.A., S.G.Buchanan, S.K.Burley, K.Conners, M.Dickey, M.Dorwart, R.Fowler, X.Gao, W.B.Guggino, W.A.Hendrickson, J.F.Hunt, M.C.Kearins, D.Lorimer, P.C.Maloney, K.W.Post, K.R.Rajashankar, M.E.Rutter, J.M.Sauder, S.Shriver, P.H.Thibodeau, P.J.Thomas, M.Zhang, X.Zhao, and S.Emtage. 2004. Structure of nucleotide-binding domain 1 of the cystic fibrosis transmembrane conductance regulator. *EMBO J* 23:282-293.

Monod,J., J.Wyman, and J.P.Changeux. 1965. On the Nature of Allosteric Transitions: A Plausible Model. *J Mol Biol* 12:88-118.

Procko,E., M.L.O'Mara, W.F.D.Bennett, D.P.Tieleman, and R.Gaudet. 2009. The mechanism of ABC transporters: general lessons from structural and functional studies of an antigenic peptide transporter. *Faseb Journal* 23:1287-1302.

Riordan,J.R., J.M.Rommens, B.Kerem, N.Alon, R.Rozmahel, Z.Grzelczak, J.Zielenski, S.Lok, N.Plavsic, J.L.Chou, and . 1989. Identification of the cystic fibrosis gene: cloning and characterization of complementary DNA. *Science* 245:1066-1073.

Smith,P.C., N.Karpowich, L.Millen, J.E.Moody, J.Rosen, P.J.Thomas, and J.F.Hunt. 2002. ATP binding to the motor domain from an ABC transporter drives formation of a nucleotide sandwich dimer. *Mol Cell* 10:139-149.

Szollosi,A., D.R.Muallem, L.Csanady, and P.Vergani. 2011. Mutant cycles at CFTR's non-canonical ATP-binding site support little interface separation during gating. *J Gen Physiol*.

Szollosi,A., P.Vergani, and L.Csanady. 2010. Involvement of F1296 and N1303 of CFTR in induced-fit conformational change in response to ATP binding at NBD2. *J Gen Physiol* 136:407-423.

Tsai,M.F., M.Li, and T.C.Hwang. 2010. Stable ATP binding mediated by a partial NBD dimer of the CFTR chloride channel. *J Gen Physiol* 135:399-414.

Vergani,P., S.W.Lockless, A.C.Nairn, and D.C.Gadsby. 2005. CFTR channel opening by ATP-driven tight dimerization of its nucleotide-binding domains. *Nature* 433:876-880.

Vergani,P., A.C.Nairn, and D.C.Gadsby. 2003. On the mechanism of MgATP-dependent gating of CFTR Cl- channels. *J Gen Physiol* 121:17-36.

Zhou,Z., X.Wang, M.Li, Y.Sohma, X.Zou, and T.C.Hwang. 2005. High affinity ATP/ADP analogues as new tools for studying CFTR gating. *J Physiol* 569:447-457.

Figure legends

Figure 1. Effects of P-ATP on rough channel gating parameters of WT CFTR. *A-B*, Macroscopic currents of prephosphorylated CFTR channels elicited by step applications (*bars*) of various concentrations of ATP (*A*) or P-ATP (*B*). *C*, Dose response curves for current stimulation by ATP (*blue symbols*) and P-ATP (*red symbols*). Mean steady currents in the presence of test nucleotide concentrations were normalized to the average of those measured in bracketing segments in the presence of 2 mM (ATP) or 32 μM (P-ATP) nucleotide. Fits to the Michaelis-Menten equation (*solid lines*) yielded K_m values shown. *D*, Steady-state current recording from a patch containing two active WT CFTR channels gating in 2 mM ATP (*blue segments*) or 10 μM P-ATP (*red segment*). *E-G*, Steady-state open probabilities (*E*), mean burst durations (*F*), and mean interburst durations (*G*) of WT CFTR in the presence of 2 mM ATP (*blue bars*) or 10 μM P-ATP (*red bars*), extracted from records with ≤2 active channels as described in Methods.

Figure 2. Steady-state mean burst duration of H1348A CFTR is insensitive to elevation of [ATP]. *A*, Steady-state current recording from a patch containing two active H1348A CFTR channels gating in 2 mM (*green segment*) or 10 mM (*dark blue segment*) ATP. *B-D*, Steady-state open probabilities (*B*), mean burst durations (*C*), and mean interburst durations (*D*) of H1348A CFTR in the presence of 2 mM (*green bars*) or 10 mM (*dark blue bars*) ATP, extracted from records with ≤5 active channels as described in Methods.

Figure 3. P-ATP and the H1348A mutation slow non-hydrolytic CFTR closure. *A*, *D*, Macroscopic currents of prephosphorylated K1250A (*A*) and E1371S (*D*) CFTR channels elicited by exposure (*bars*) to either 10 mM ATP alternating with 50 μM P-ATP (*A*) or 2 mM ATP alternating with 10 μM P-ATP (*D*); the 5-fold higher nucleotide concentrations for the K1250A constructs were used to compensate for the large decrease in apparent ATP affinity caused by this mutation (Vergani et al., 2003). Current decay time courses following sudden removal of the nucleotide were fitted with single exponentials (*colored solid lines*), colored numbers are time constants (in ms) which reflect mean burst durations. *B*, *E*, Macroscopic currents of prephosphorylated K1250A/H1348A (*B*) and E1371S/H1348A (*E*) CFTR

channels elicited by transient exposure (*bars*) to either 10 mM (*B*) or 2 mM (*E*) ATP. Current decay time courses following sudden ATP removal were fitted with double exponentials (*colored solid lines*), colored numbers are calculated average burst durations (τ*, in ms; see Methods). The fit parameters were τ_1=37 s, τ_2=165 s, A_1=0.34, A_2=0.66 for panel *B*, and τ_1=24 s, τ_2=179 s, A_1=0.07, A_2=0.93 for panel *E*. *C*, *F*, Non-hydrolytic closing rates of channels opened by ATP (*blue bars*) or P-ATP (*red bars*), or of channels bearing the H1348A mutation opened by ATP (*green bars*), measured in the K1250A (*C*) or E1371S (*F*) background. Closing rates were calculated as the inverse of the decay time constant following nucleotide removal; for traces which were not well fit by a single exponential average closing rate was calculated as 1/τ*.

Figure 4. Mutation H1348A and deletion of segment 415-432 (ΔRI) abolish the effect of P-ATP on hydrolytic channel closure. *A*, *D*, Steady-state recordings of single-channel currents in the presence of 2 mM ATP (*green segments*) or 10 μM P-ATP (*brown segments*) for H1348A (*A*) or ΔRI CFTR (*D*). *Insets* show at an expanded time scale 10-s intervals taken from the stable steady section of each segment (*gray bars*). In *A* V_m was -40 mV. *B*, *E*, Closing rates, obtained as the inverses of the steady-state mean burst duration, for H1348A (*B*) and ΔRI (*E*) CFTR channels gating in ATP (*green bars*) or P-ATP (*brown bars*). Steady-state closing rates of WT CFTR in ATP (*blue bars*) and P-ATP (*red bars*) were extracted from the data shown in Fig. 1F. *C*, *F*, Thermodynamic mutant cycles built on (hydrolytic) closing rates for the interaction of the P-ATP P-group with residue 1348 (*C*), or the RI region (*F*). Each corner is represented by the particular site-1 protein structure (H or A at position 1348 (*C*); maintained or deleted RI (*F*)) and the nucleotide driving gating (ATP or P-ATP), respectively. $\Delta\Delta G^{\ddagger}$ values (mean±S.E.M.) on arrows show perturbation-induced changes in the stability of the closing transition state with respect to the open ground state, and were used to calculate (see Methods) the coupling energy for the P-group – 1348 (*C*) and the P-group – RI (*F*) interaction ($\Delta\Delta G_{int\ (closing)}$).

Figure 5. Mutation H1348A and deletion of segment 415-432 (ΔRI) potentiate the effect of P-ATP on non-hydrolytic channel closure. *A*, *D*, Macroscopic currents from K1250A/H1348A (*A*) and

K1250A/ΔRI (*D*) CFTR channels elicited by exposures to 10 mM ATP or 50 μM P-ATP (*bars*). *Solid lines* are single-exponential fits to the current relaxation time courses following nucleotide removal, with time constants indicated. *B*, *E*, Non-hydrolytic closing rates for K1250A/H1348A (*B*) and K1250A/ΔRI (*E*) CFTR channels, obtained as the inverses of the relaxation time constants following removal of ATP (*green bars*) or P-ATP (*brown bars*); closing rates of K1250A CFTR following removal of ATP (*blue bars*) and P-ATP (*red bars*) were replotted from Fig. 3C. *C*, *F*, Thermodynamic mutant cycles built on non-hydrolytic closing rates for the interaction of the P-ATP P-group with residue 1348 (*C*), or the RI region (*F*). Each corner is represented by the particular site-1 protein structure (H or A at position 1348 (*C*); maintained or deleted RI (*F*)) and the nucleotide driving gating (ATP or P-ATP), respectively. $\Delta\Delta G^{\ddagger}$ values (mean±S.E.M.) on arrows show perturbation-induced changes in the stability of the transition state for non-hydrolytic closure with respect to the open ground state, and were used to calculate the coupling energy for the P-group – 1348 (*C*) and the P-group – RI (*F*) interaction ($\Delta\Delta G_{int\ (closing)}$).

Figure 6. Relaxation time courses of macroscopic WT, H1348A, and ΔRI CFTR currents upon sudden nucleotide removal. *A*-*C*, Macroscopic currents of prephosphorylated WT (*A*), H1348A (*B*), and ΔRI (*C*) CFTR channels elicited by exposure (*bars*) to either 2 mM ATP alternating with 10 μM P-ATP (*A*, *C*), or 2 mM ATP alternating with either 10 mM ATP (*B*, *top*) or 10 μM P-ATP (*B*, *bottom*). Current decay time courses following sudden removal of the nucleotide were fitted with single exponentials (*colored solid lines*), colored numbers are time constants (in ms). *D*, Closing time constants of WT CFTR currents upon removal of 2 mM ATP (*blue bar*) or 10 μM P-ATP (*red bar*), of H1348A CFTR currents upon removal of 2 (*left green bar*) or 10 mM ATP (*dark blue bar*) or 10 μM P-ATP (*left brown bar*), and of ΔRI CFTR currents upon removal of 2 mM ATP (*right green bar*) or 10 μM P-ATP (*right brown bar*). As a comparison, *striped bars* replot mean burst durations of the respective constructs measured at steady state in the presence of the respective nucleotide (from Figs. 1F, 2C, and 4E).

Figure 7. P-ATP and the H1348A mutation slow the $O_1 \rightarrow O_2$ transition of CFTR channels. *A-B*, Histograms of open burst durations compiled from 621 open burst events of single WT CFTR channels gating in 10 μM P-ATP (*A*) and from 908 open burst events of single H1348A CFTR channels gating in 2 mM ATP (*B*). Both distributions were fitted by maximum likelihood to either a single exponential (*blue dotted lines*) or to the Scheme in panel *C* with rate k_{-1} fixed to zero (*red lines*); the latter fits proved significantly ($P<0.01$ for *A*, $P\approx0.05$ for *B*) better by the log-likelihood ratio test. Fit parameters, as well as calculated time constants and fractional amplitudes of the exponential components of the fitted distributions are plotted in both panels. *Insets*, 30-s segments of single-channel recordings. *C*, Simplified cyclic gating scheme (from (Csanády et al., 2010)) used for maximum likelihood fitting of open burst distributions, depicting closed and open states with either ATP (states C_1 and O_1), or ADP (states C_2 and O_2) bound at site 2. Pore opening/closure is assumed quasi-simultaneous with formation/disruption of the NBD dimer. TMDs, *cyan rectangles*; NBD1, *green*; NBD2, *blue*; ATP, *yellow*; ADP, *red*. *D*, Summary of rates k_1 and k_2 obtained from the fits in *A* and *B* for WT CFTR gating in 10 μM P-ATP (*red bars*) and H1348A CFTR gating in 2 mM ATP (*green bars*); as a comparison, the values measured for WT CFTR gating in 2 mM ATP (*blue bars*) are replotted from (Csanády et al., 2010). Error bars represent 0.5-unit loglikelihood intervals. Note, that in the presence of the site-1 perturbations rate k_2 could be estimated only to a limited precision, due to the increased discrepancy between the values of k_1 and k_2 (cf. (Csanády, 2006); k_2/k_1 is 11, 18, and 29, respectively, for WT+ATP, WT+P-ATP, and H1348A+ATP)

Figure 8. Energetic interpretation of the gating effects of P-ATP and the H1348A mutation. Free energy profiles (*top*, not drawn to scale) of channels moving sequentially through the gating states depicted below (from Fig. 7C), in the absence (*blue energy profile*) or presence (red energy profile) of a perturbation (*red star* in cartooned states) in composite site 1. A selective stabilization of the O_1 ground state (by $\delta\Delta G_{O1}$, relative to both C_1 and O_2) is predicted to increase the heights of the free energy barriers for exiting O_1 in both directions ($\Delta G^{\ddagger}_{-1}$ and $\Delta G^{\ddagger}_{1}$; compare *red* and *blue* vertical double arrows), thereby slowing both rate k_1 and k_{-1} (cartoon).

Figure 9. Partial separation of degenerate site in an asymmetrical bacterial ABC exporter. Ribbon diagram of NBD dimer from the crystal structure of TM287/288 (PDBID: 3QF4) with AMPPNP (*yellow*) bound at the degenerate site. Conserved Walker A threonines (T368 in TM287, T390 in TM288; *red*), as well as D-loop residue N521 of TM288 and corresponding TM287 residue S499 (*violet*) are highlighted in spacefill. The empty active site is wide open, while the nucleotide-bound degenerate site retains some contact between the two NBD surfaces through opposing Walker A and D-loop motifs. NBD color coding follows that used in Fig. 7C: TM287, *green*; TM288, *blue*.

Fig. 1

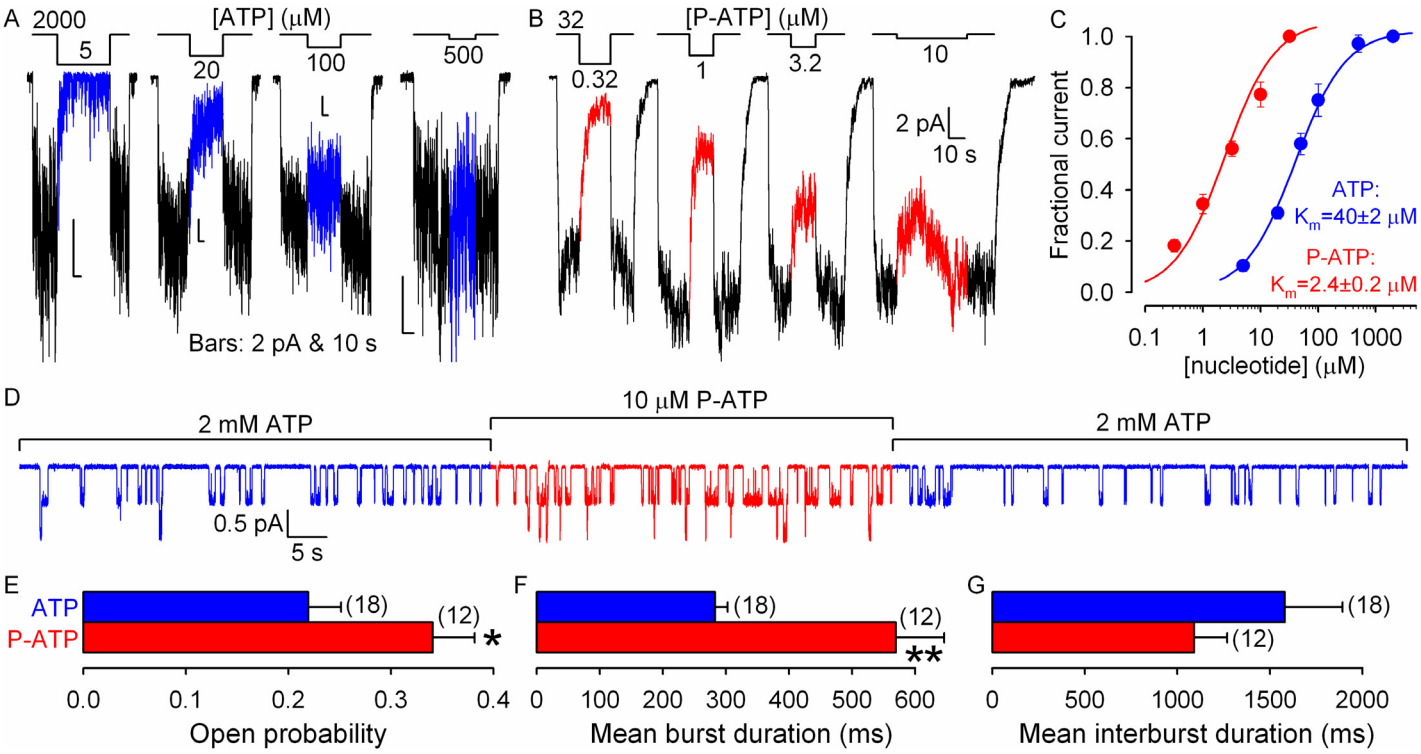
A
2000
[ATP] (μM)
5
20
100
500
Bars: 2 pA & 10 s
B
32
[P-ATP] (μM)
0.32
1
3.2
10
2 pA
10 s
C
Fractional current
1.0
0.8
0.6
0.4
0.2
0.0
ATP:
Km=40±2 μM
P-ATP:
Km=2.4±0.2 μM
0.1
1
10
100
1000
[nucleotide] (μM)
D
2 mM ATP
10 μM P-ATP
2 mM ATP
0.5 pA
5 s
E
ATP
P-ATP
(18)
(12)
*
0.0
0.1
0.2
0.3
0.4
Open probability
F
(18)
(12)
**
0
100
200
300
400
500
600
Mean burst duration (ms)
G
(18)
(12)
0
500
1000
1500
2000
Mean interburst duration (ms)

Fig. 2

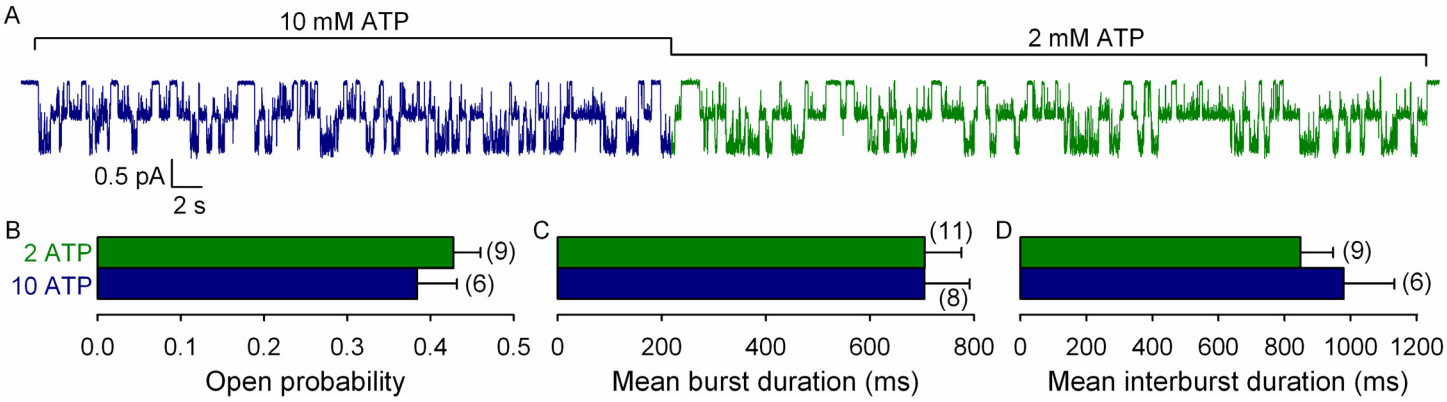
A
10 mM ATP
2 mM ATP
0.5 pA
2 s
B
2 ATP
10 ATP
(9)
(6)
0.0
0.1
0.2
0.3
0.4
0.5
Open probability
C
(11)
(8)
0
200
400
600
800
Mean burst duration (ms)
D
(9)
(6)
0
200
400
600
800
1000
1200
Mean interburst duration (ms)

Fig. 3

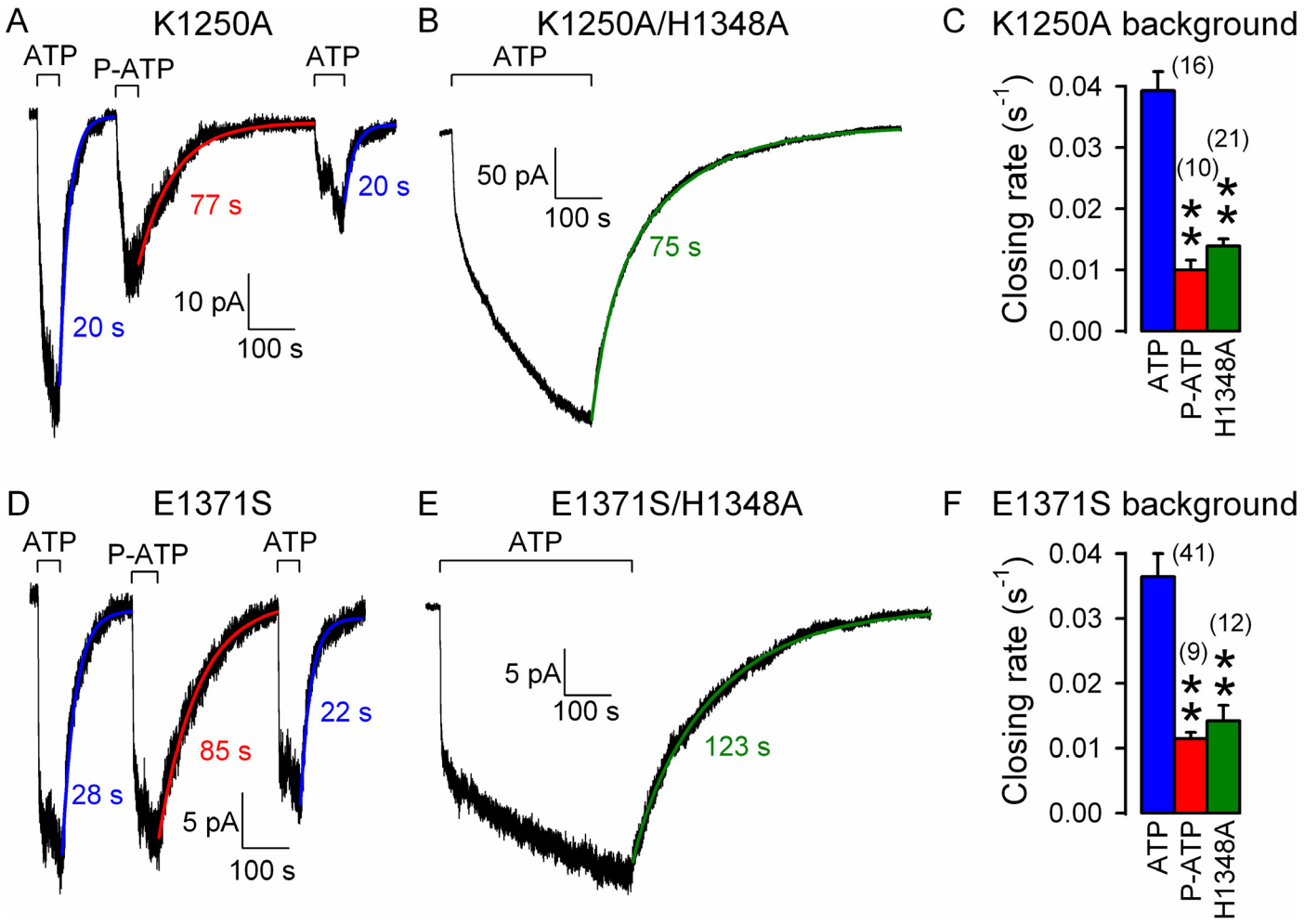
A
K1250A
ATP
P-ATP
ATP
77 s
20 s
20 s
10 pA
100 s
B
K1250A/H1348A
ATP
50 pA
100 s
75 s
C
K1250A background
Closing rate (s-1)
0.04
0.03
0.02
0.01
0.00
(16)
(10)
(21)
**
**
ATP
P-ATP
H1348A
D
E1371S
ATP
P-ATP
ATP
28 s
85 s
22 s
5 pA
100 s
E
E1371S/H1348A
ATP
5 pA
100 s
123 s
F
E1371S background
Closing rate (s-1)
0.04
0.03
0.02
0.01
0.00
(41)
(9)
(12)
**
**
ATP
P-ATP
H1348A

Fig. 4

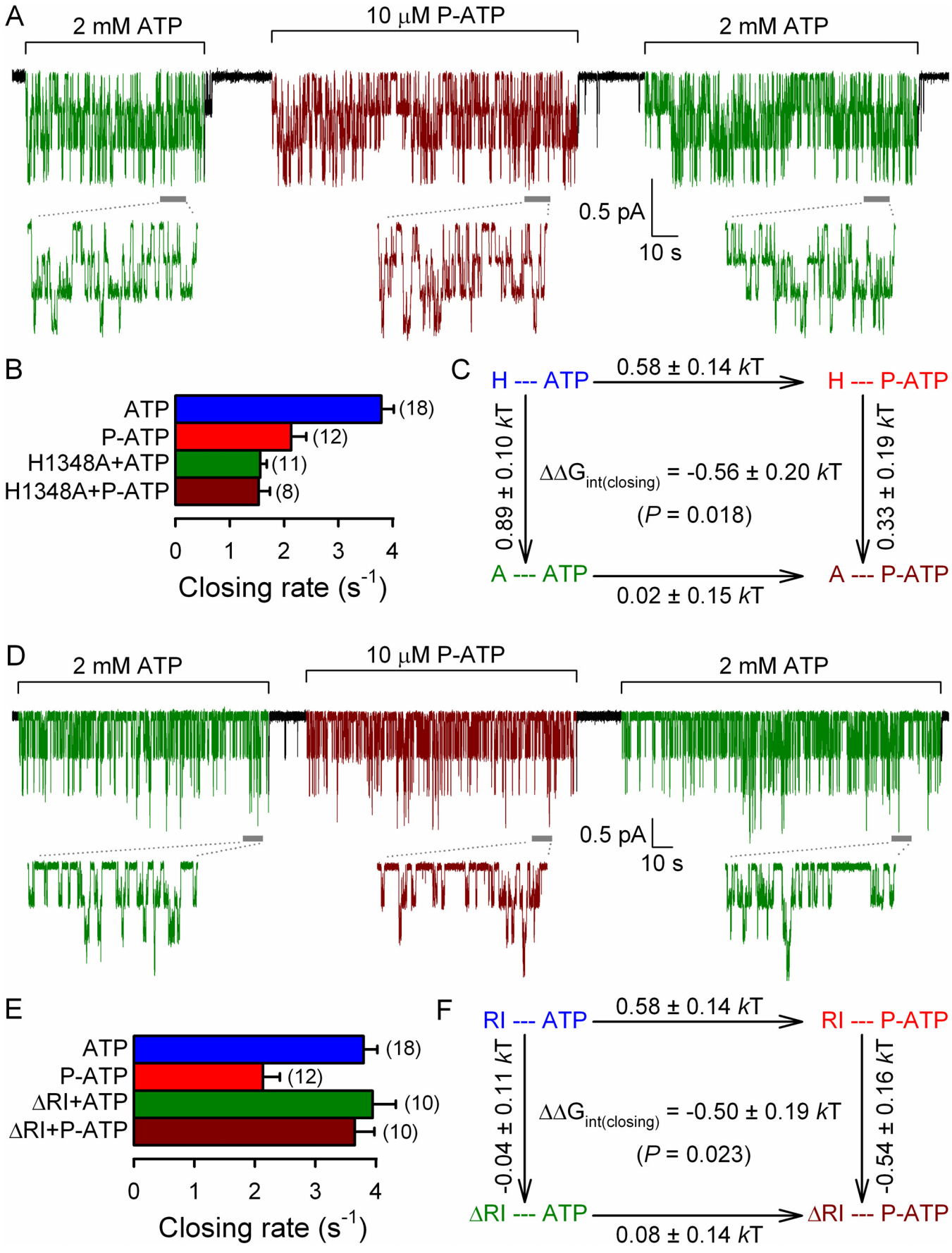
A
2 mM ATP
10 μM P-ATP
2 mM ATP
0.5 pA
10 s
B
ATP
P-ATP
H1348A+ATP
H1348A+P-ATP
(18)
(12)
(11)
(8)
0
1
2
3
4
Closing rate (s-1)
C
H --- ATP
0.58 ± 0.14 kT
H --- P-ATP
0.89 ± 0.10 kT
ΔΔGint(closing) = -0.56 ± 0.20 kT
(P = 0.018)
0.33 ± 0.19 kT
A --- ATP
0.02 ± 0.15 kT
A --- P-ATP
D
2 mM ATP
10 μM P-ATP
2 mM ATP
0.5 pA
10 s
E
ATP
P-ATP
ΔRI+ATP
ΔRI+P-ATP
(18)
(12)
(10)
(10)
0
1
2
3
4
Closing rate (s-1)
F
RI --- ATP
0.58 ± 0.14 kT
RI --- P-ATP
-0.04 ± 0.11 kT
ΔΔGint(closing) = -0.50 ± 0.19 kT
(P = 0.023)
-0.54 ± 0.16 kT
ΔRI --- ATP
0.08 ± 0.14 kT
ΔRI --- P-ATP

Fig. 5

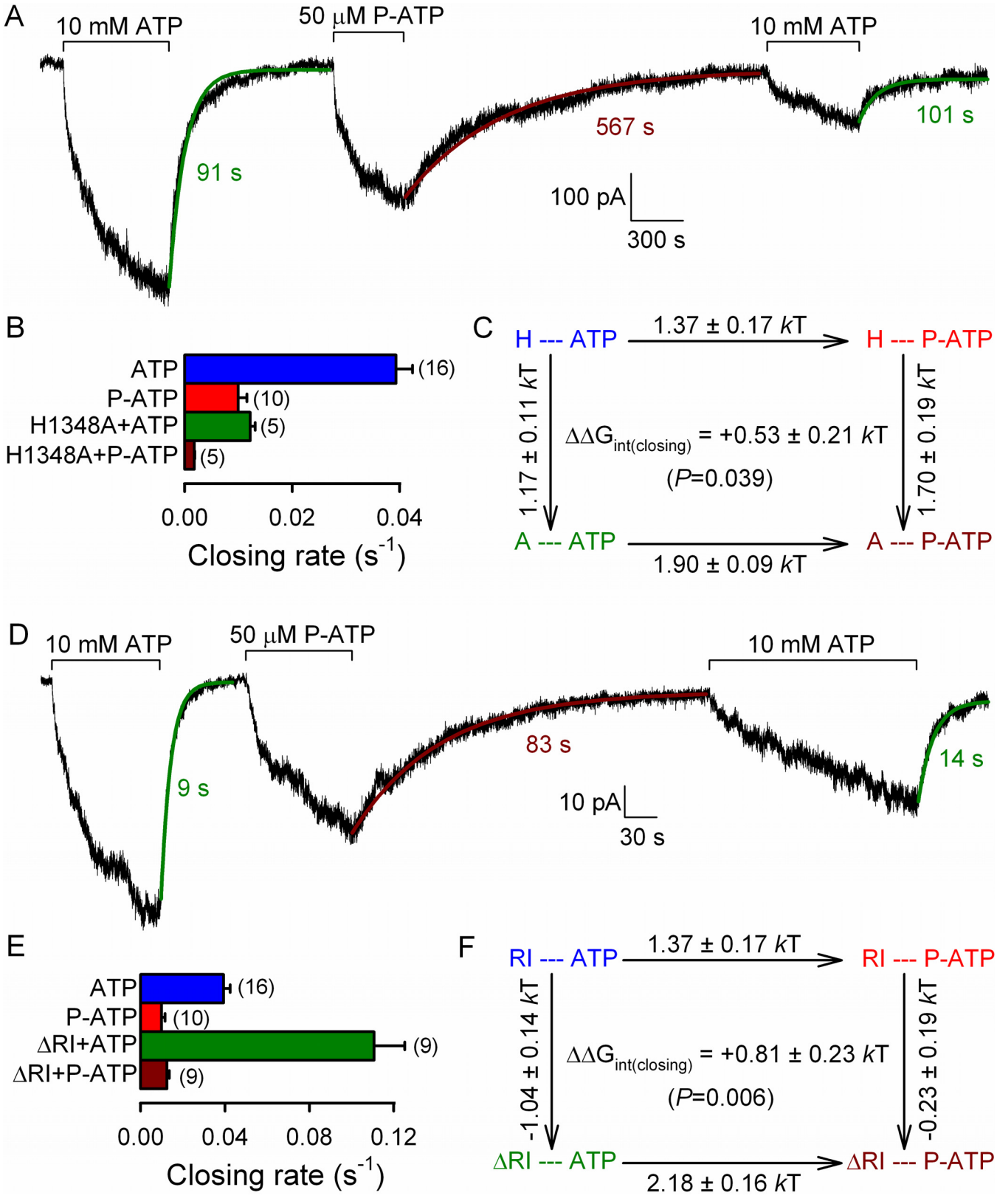
A
10 mM ATP
50 μM P-ATP
10 mM ATP
91 s
567 s
101 s
100 pA
300 s
B
ATP
P-ATP
H1348A+ATP
H1348A+P-ATP
(16)
(10)
(5)
(5)
0.00
0.02
0.04
Closing rate (s-1)
C
H --- ATP
1.37 ± 0.17 kT
H --- P-ATP
1.17 ± 0.11 kT
ΔΔGint(closing) = +0.53 ± 0.21 kT
(P=0.039)
1.70 ± 0.19 kT
A --- ATP
1.90 ± 0.09 kT
A --- P-ATP
D
10 mM ATP
50 μM P-ATP
10 mM ATP
9 s
83 s
14 s
10 pA
30 s
E
ATP
P-ATP
ΔRI+ATP
ΔRI+P-ATP
(16)
(10)
(9)
(9)
0.00
0.04
0.08
0.12
Closing rate (s-1)
F
RI --- ATP
1.37 ± 0.17 kT
RI --- P-ATP
-1.04 ± 0.14 kT
ΔΔGint(closing) = +0.81 ± 0.23 kT
(P=0.006)
-0.23 ± 0.19 kT
ΔRI --- ATP
2.18 ± 0.16 kT
ΔRI --- P-ATP

Fig. 6

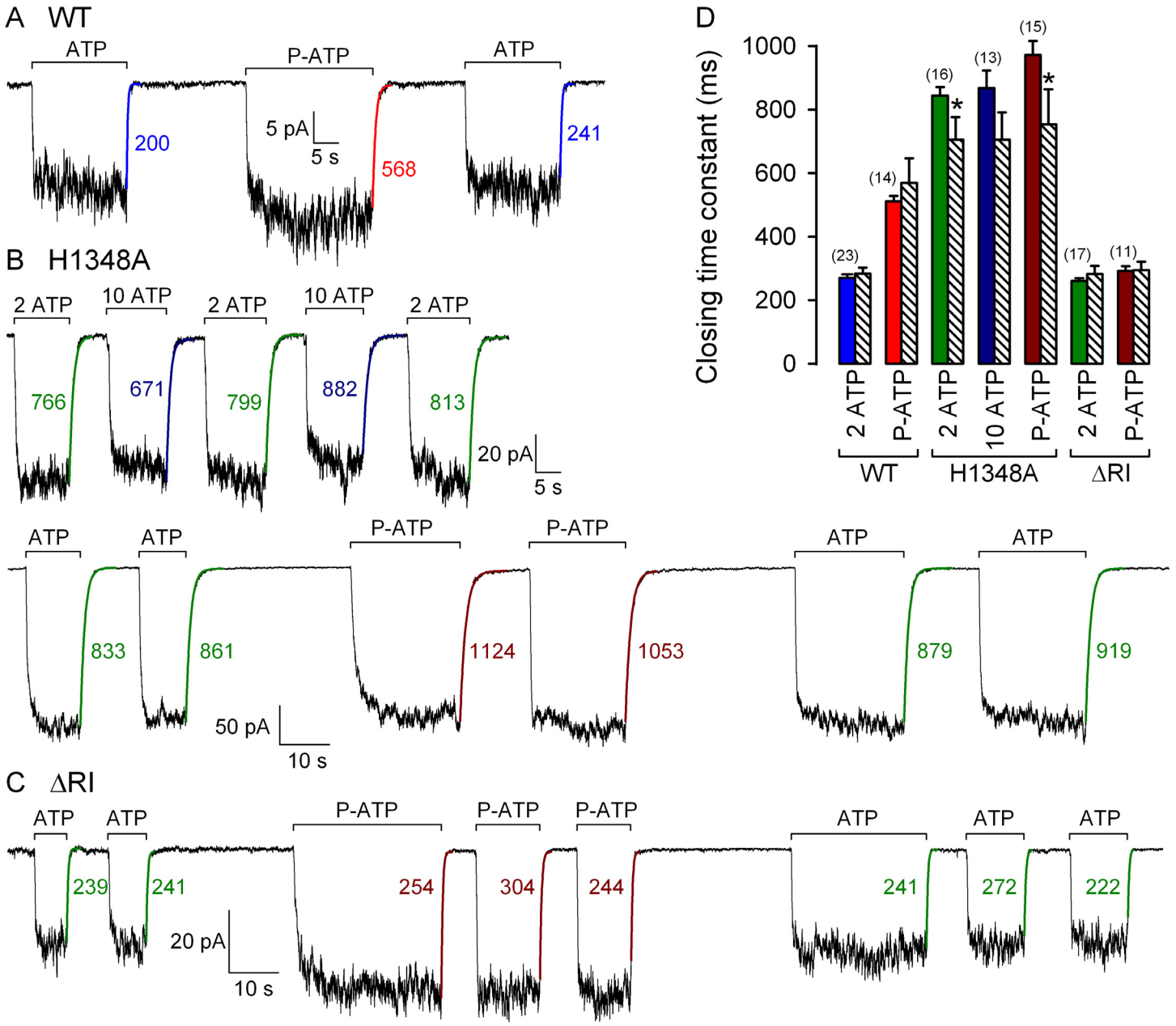
A WT
ATP
P-ATP
ATP
200
5 pA
5 s
568
241
B H1348A
2 ATP
10 ATP
2 ATP
10 ATP
2 ATP
766
671
799
882
813
20 pA
5 s
ATP
ATP
P-ATP
P-ATP
ATP
ATP
833
861
1124
1053
879
919
50 pA
10 s
C ΔRI
ATP
ATP
P-ATP
P-ATP
P-ATP
ATP
ATP
ATP
239
241
254
304
244
241
272
222
20 pA
10 s
D
Closing time constant (ms)
1000
800
600
400
200
0
(23)
(14)
(16)
(13)
(15)
(17)
(11)
*
*
2 ATP
P-ATP
2 ATP
10 ATP
P-ATP
2 ATP
P-ATP
WT
H1348A
ΔRI

Fig. 7

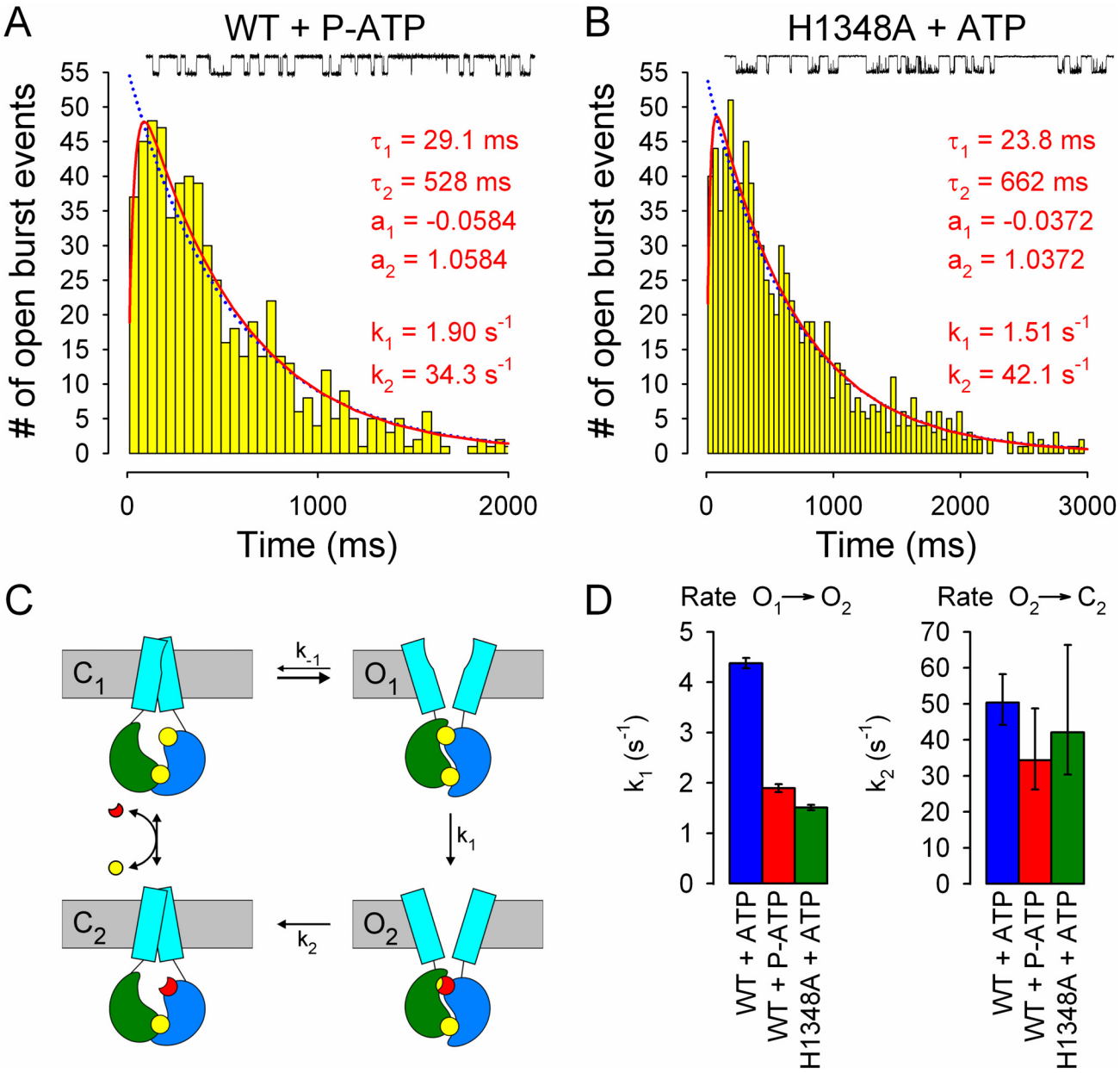
A
WT + P-ATP
# of open burst events
Time (ms)
τ1 = 29.1 ms
τ2 = 528 ms
a1 = -0.0584
a2 = 1.0584
k1 = 1.90 s-1
k2 = 34.3 s-1
B
H1348A + ATP
# of open burst events
Time (ms)
τ1 = 23.8 ms
τ2 = 662 ms
a1 = -0.0372
a2 = 1.0372
k1 = 1.51 s-1
k2 = 42.1 s-1
C
C1
O1
C2
O2
k-1
k1
k2
D
Rate O1→O2
k1 (s-1)
Rate O2→C2
k2 (s-1)
WT + ATP
WT + P-ATP
H1348A + ATP

Fig. 8

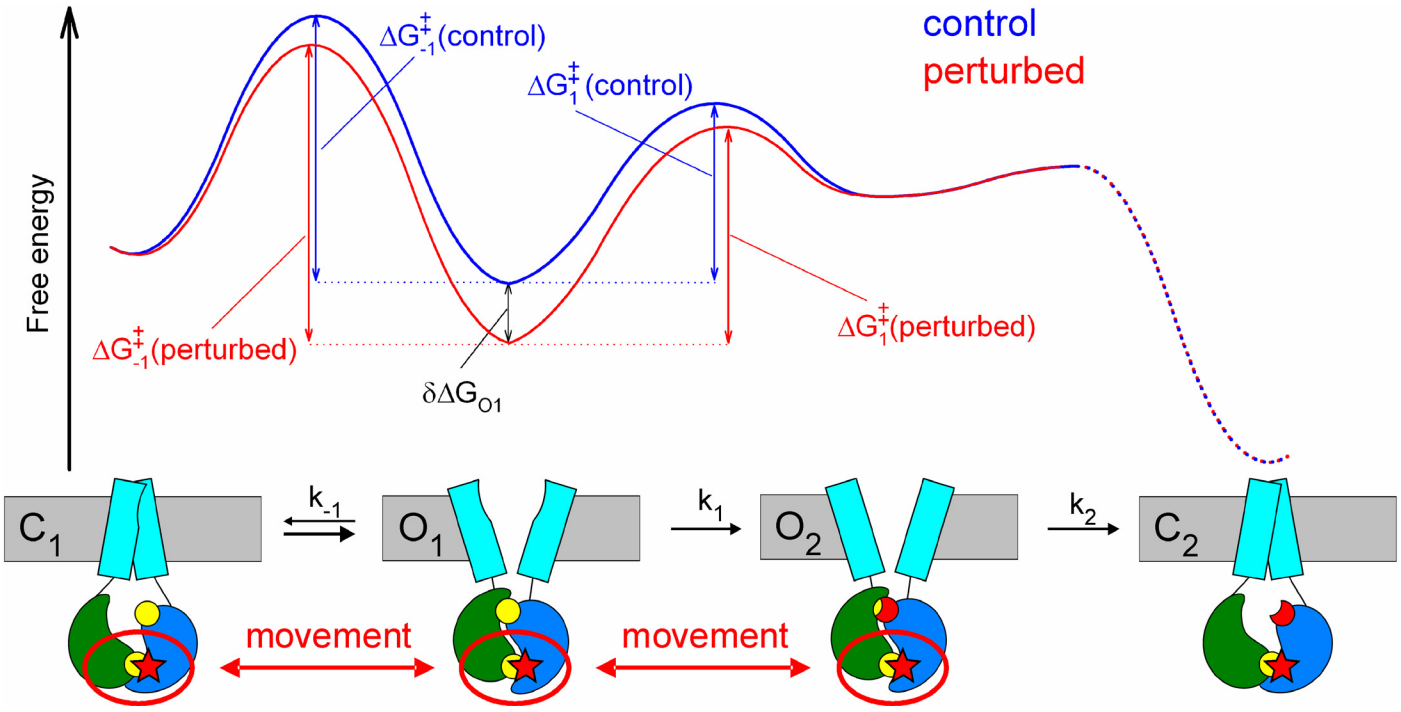
Free energy
control
perturbed
$\Delta G^{\ddagger}_{-1}$(control)
$\Delta G^{\ddagger}_{1}$(control)
$\Delta G^{\ddagger}_{-1}$(perturbed)
$\Delta G^{\ddagger}_{1}$(perturbed)
$\delta\Delta G_{O1}$
C_1
k_{-1}
O_1
k_1
O_2
k_2
C_2
movement
movement

Fig. 9

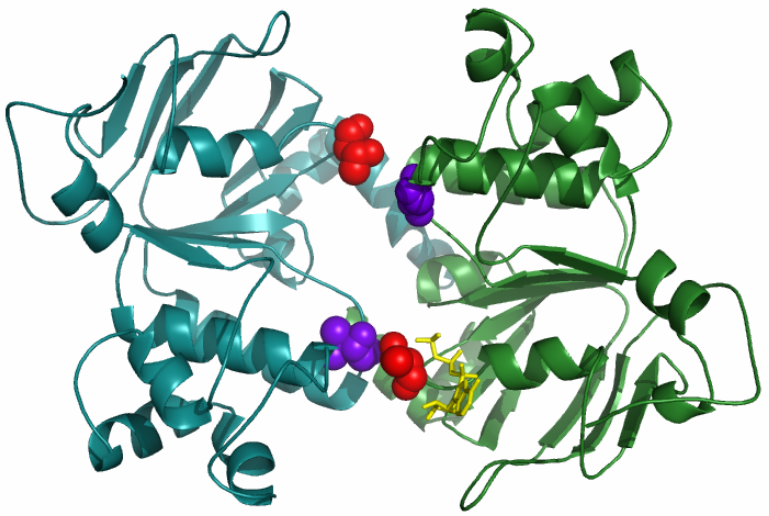

Fig. S1

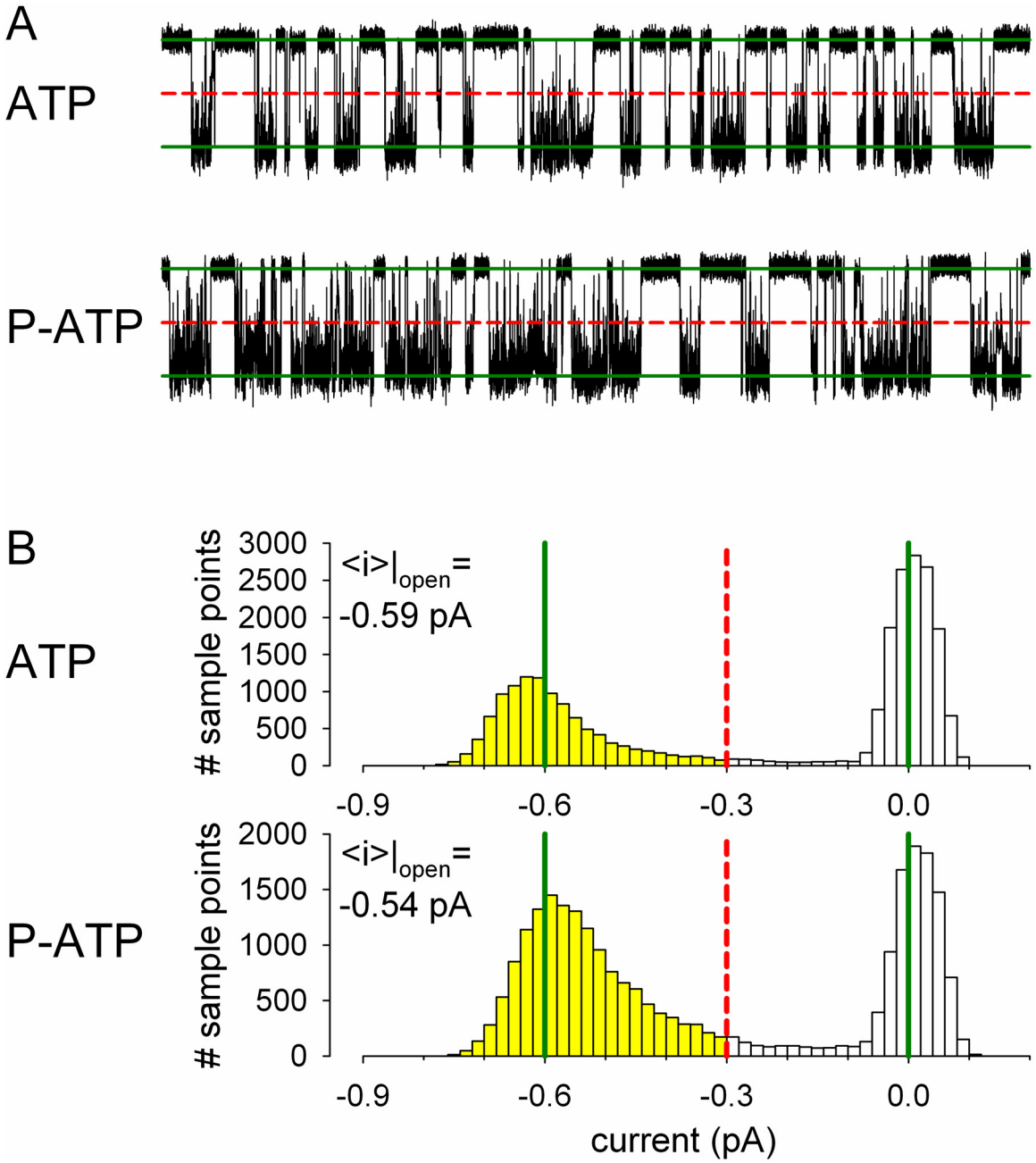

Figure S1. Average unitary conductance is smaller for channels opened by P-ATP. *A,* 25-s segments of recording of a single WT CFTR channel gating first in ATP (*top*) and then in P-ATP (*bottom*); V_m=-80 mV. *Solid green lines*, conductance levels used for idealization; *dotted red line*, half-amplitude threshold. *B*, Amplitude histograms for the segments of record shown in *A*. Bins corresponding to data points above the idealization threshold (*red dotted lines*) are highlighted in yellow. Average currents for such data points (i.e., during idealized "open" events) are plotted in each panel.

Fig. S2

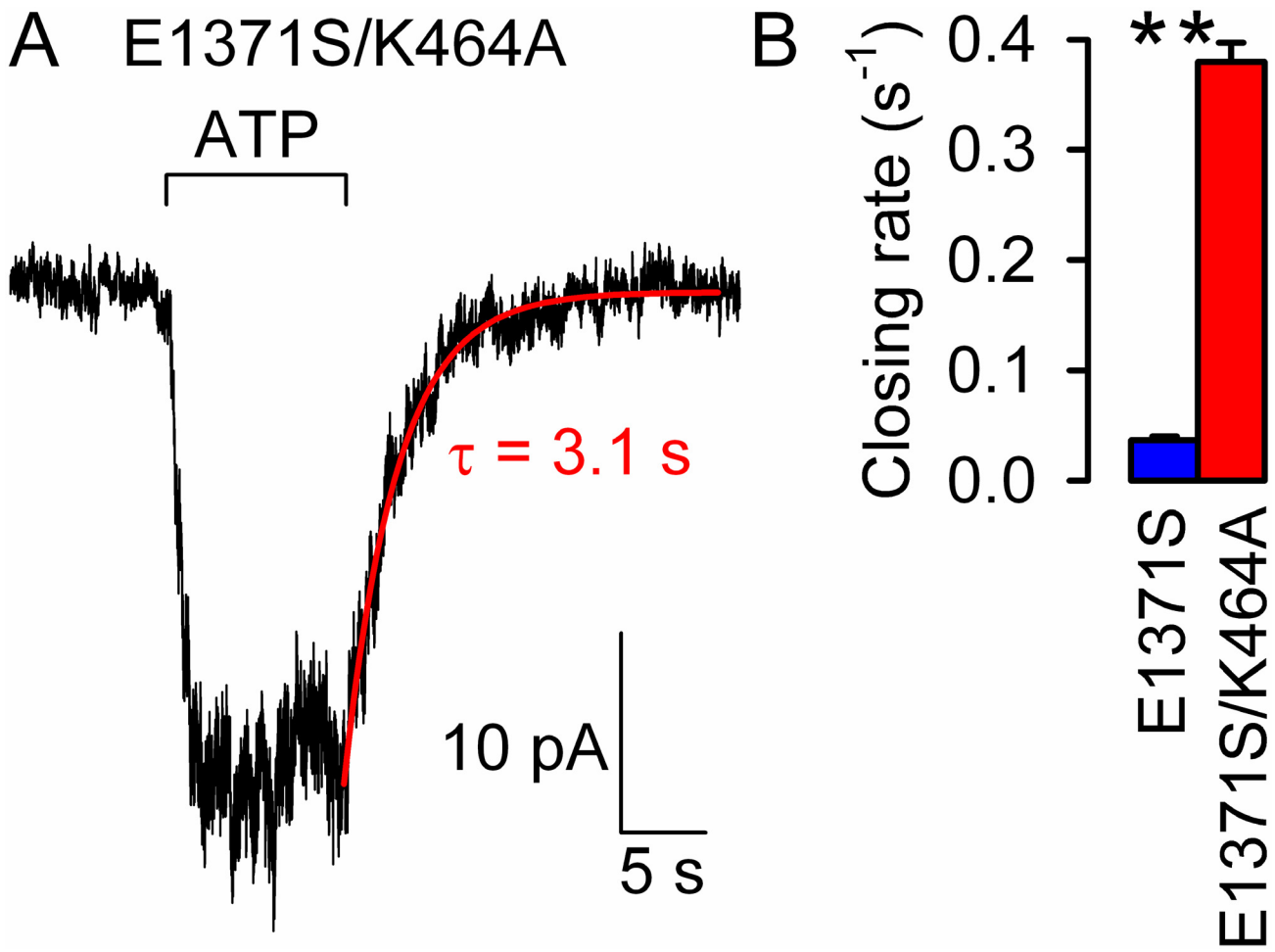

Figure S2. The K464A mutation accelerates non-hydrolytic closure of E1371S CFTR. *A*, Macroscopic current of prephosphorylated E1371S/K464A CFTR channels elicited by transient exposure (*bar*) to 10 mM ATP. Current decay time course following sudden ATP removal was fitted with a single exponential (*red solid line*); time constant (in ms) reflects mean burst duration. *B*, Non-hydrolytic closing rate of E1371S/K464A (*red bar*), calculated as the inverse of the decay time constant following ATP removal. As a comparison, E1371S closing rate (*blue bar*) is replotted from Fig. 3F.